

www.acsami.org Research Article

Buckle-Delamination-Enabled Stretchable Silver Nanowire Conductors

Shuang Wu, Shanshan Yao, Yuxuan Liu, Xiaogang Hu, He Helen Huang, and Yong Zhu*



Cite This: ACS Appl. Mater. Interfaces 2020, 12, 41696-41703



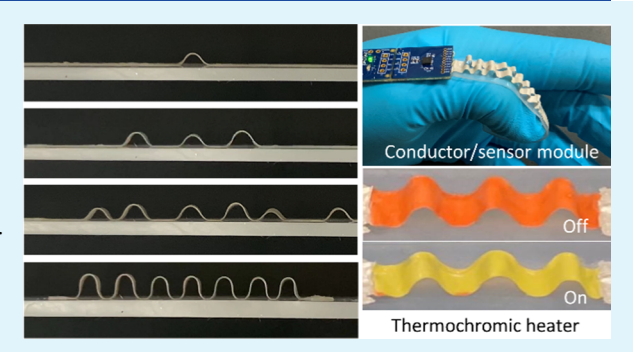
ACCESS I

Metrics & More



Supporting Information

ABSTRACT: Controlled buckling and delamination of thin films on a compliant substrate has attracted much attention for applications ranging from micro/nanofabrication to flexible and stretchable electronics to bioengineering. Here, a highly conductive and stretchable conductor is fabricated by attaching a polymer composite film (with a thin layer of silver nanowires embedded below the surface of the polymer matrix) on top of a prestretched elastomer substrate followed with releasing the prestrain. A partially delaminated wavy geometry of the polymer film is created. During the evolution of the buckledelamination, the blisters pop-up randomly but self-adjust into a uniform distribution, which effectively reduces the local strain in the silver nanowires. The resistance change of the conductor is less than 3%



with the applied strain up to 100%. A theoretical model on the buckle-delamination structure is developed to predict the geometrical evolution, which agrees well with experimental observation. Finally, an integrated silver nanowire/elastomer sensing module and a stretchable thermochromic device are developed to demonstrate the utility of the stretchable conductor. This work highlights the important relevance of mechanics-based design in nanomaterial-enabled stretchable devices.

KEYWORDS: stretchable conductor, silver nanowire, buckling, buckle-delamination, wrinkling, thermochromic

■ INTRODUCTION

The field of stretchable electronics has evolved rapidly in the past decade. Stretchable electronics has significantly broadened the applications of conventional electronics to new areas such as continuous health monitoring, human—machine interfaces, and electronic skin in robotics and prosthetics. Stretchable conductors, as the most fundamental building blocks of stretchable electronics, have attracted loads of attention. There are two main strategies to develop stretchable conductors based on the materials used: nanocomposites with synthesized nanomaterials dispersed into a polymer matrix and deposited thin films exploiting mechanically guided structural design. Other strategies include using liquid metals patterned and encapsulated into channels of elastomer substrates.

For the nanocomposite strategy, a wide variety of nanomaterials have been employed such as metal nanoparticles, ¹⁷ nanowires, ^{7,18} nanoflakes, ¹⁹ carbon nanotubes, ^{10–12} and graphene. ²⁰ A number of low-cost, scalable printing, or solution-processed methods have been developed recently to deposit and pattern the nanomaterials. ²¹ The key to this strategy is in maintaining the conductive percolation pathways when the substrate or matrix is stretched. Several approaches, such as using ultralong nanowires and hybrids of different types of nanomaterials, ^{22,23} were exploited to enhance and maintain the conductivity. Despite the exciting progress, the

conductivity of such composites typically drops with increasing strain applied to the substrate/matrix. On the other hand, the structural design strategy can significantly reduce the effective strain on the conductors, leading to nearly constant conductivity irrespective of the applied strain. However, so far this strategy has been mainly applied to the deposited thin films, relying on costly microfabrication processes (e.g., vacuum deposition and photolithography). It would be interesting to exploit the structural design strategy for the nanocomposites.

A number of mechanically guided structural designs have been reported, such as wrinkles, buckling-driven delamination, serpentines, 2D spirals, 3D helices, and kirigami. 15,24–28 When a bilayer structure consisting of a stiff thin film and a soft substrate is compressed, there are two typical modes of buckling instability, wrinkling and buckling-driven delamination, corresponding to strong and weak interfacial bonding. The stretchability offered by wrinkling is relatively small (<20%). Recently, buckle-delamination has gained growing

Received: May 28, 2020 Accepted: August 18, 2020 Published: August 18, 2020





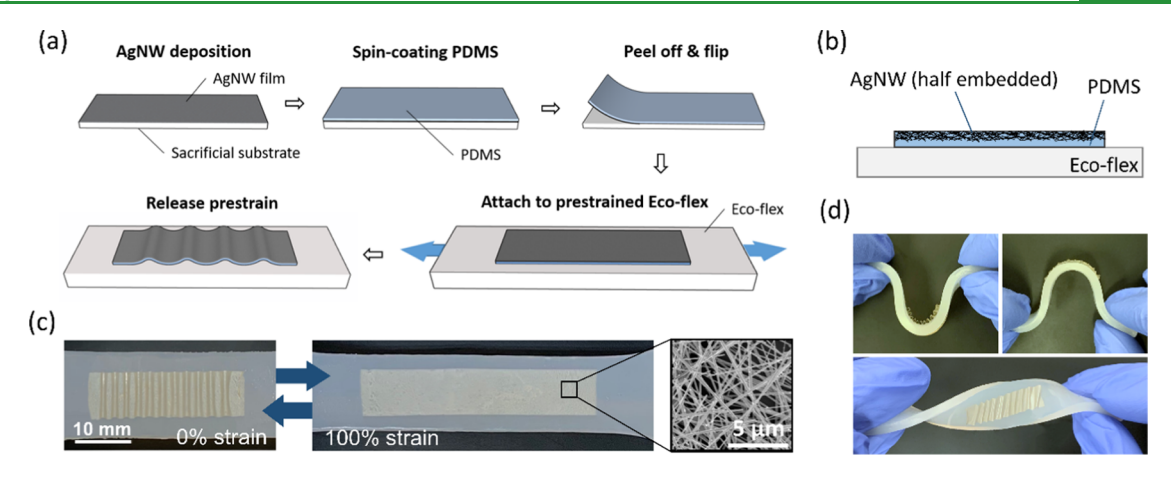


Figure 1. (a) Schematic illustrations of the fabrication process of the buckle-delamination-enabled stretchable conductor. (b) Schematic cross-sectional view of the stretchable conductor showing the AgNWs just below the PDMS surface (not to scale). Note that the AgNW/PDMS composite layer is much thinner than the pure PDMS layer. (c) Photographs of the stretchable conductor stretched from 0 to 100% in the longitudinal direction and the SEM image showing the top surface of the conductor. (d) Photographs of the stretchable AgNW conductor bended and twisted.

interest. By creating selective bonding sites between the film and the substrate, periodic delamination patterns have been formed for stretchable electronics, where the peak strain in the film can be two orders of magnitude smaller than the applied strain. ^{27,30} Another type of buckle-delamination, spontaneous buckle-delamination, has been recently reported. ^{31,32} Compared to the constrained buckle-delamination, the spontaneous buckle-delamination is simple and does not require the complex procedure of defining the adhesion site lithographically.

Here, for the first time, we report exploiting the spontaneous buckle-delamination for nanocomposite-based stretchable conductors. The stretchable conductor was fabricated by bonding a silver nanowire/poly(dimethylsiloxane) (AgNW/PDMS) composite film onto a prestrained Eco-flex substrate. After releasing the prestrain, the spontaneous delamination was generated. The mechanical model was developed to predict the geometrical evolution, which agreed well with the experimental observation. The electric performance was tested with cycle loading. Finally, an integrated AgNW/elastomer module and a stretchable thermochromic device were demonstrated to illustrate the utility of the stretchable conductor.

■ RESULTS AND DISCUSSION

Figure 1a illustrates the fabrication processes of the stretchable conductor. First, AgNW solution was drop cast onto a sacrificial substrate. After the solvent was evaporated, AgNWs were randomly distributed to form a percolation network. A thin layer of poly(dimethylsiloxane) (PDMS) was spin-coated on top of the AgNW network and cured at room temperature. After curing, AgNWs were embedded just below the surface of PDMS (Figure 1b). Then, the AgNW/PDMS composite film was peeled off from the sacrificial substrate and attached to a prestretched Eco-flex ribbon by van der Waals forces. Finally, releasing the prestrain on the Eco-flex substrate rendered the AgNW/PDMS composite film partially delaminated from the substrate in a periodic wavy form. In addition to stretching, the AgNW/PDMS/Eco-flex structure was stable under bending and twisting (Figure 1d).

The instability of a thin film bonded to a substrate under compression has been well studied.²⁹ As the compressive strain increases beyond a critical value, the thin film starts to wrinkle,

showing a sinusoidal shape, which evolves to localized buckling-driven delamination under increasing compression. 13,33,34 As illustrated in Figure 1a, a uniaxial tensile prestrain $\varepsilon_{\rm pre}$ on the Eco-flex substrate was applied. Then, a stress-free AgNW/PDMS composite film with length L_0 (1 + $\varepsilon_{\rm pre}$) was attached onto the Eco-flex substrate. When the prestrain was released, the substrate underwent a compressive strain $\varepsilon_{\rm apply}$ increasing from 0 to $-1/(1+\varepsilon_{\rm pre})$. As the compressive strain gradually increased, a 1-D periodic buckledelamination structure was generated, as shown in Figure 1c.

Figure 2a shows the top-view and side-view optical images of the buckle-delamination process when a 100% prestrain

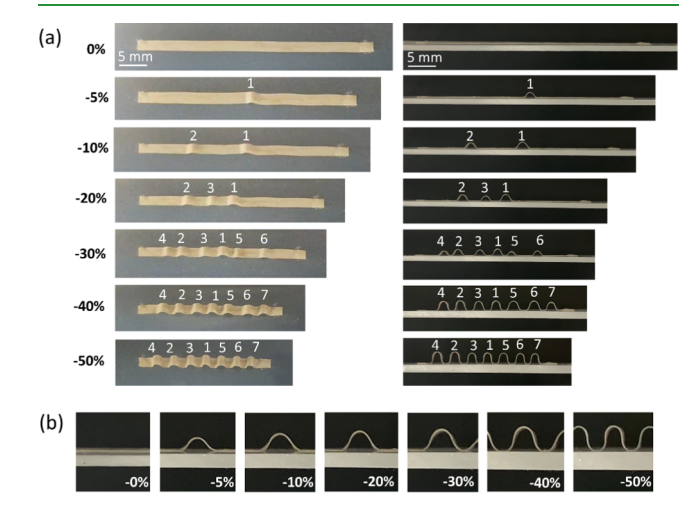


Figure 2. (a) Photographs of the stretchable AgNW conductor under compressive strain (0-50%) from both top view and side view. (b) Photographs tracing the first delaminated blister from 0% strain to -50% strain.

(equivalent compressive strain $\varepsilon_{\rm apply}$ of -50%) was released gradually. Periodic delamination of the AgNW/PDMS film occurred sequentially. The delaminated buckles or blisters popped up one by one with the increasing compressive strain. From the experiment, we can observe that the location of each blister and the sequence of blister popping up are random and not repeatable, under repeated stretching and

releasing of the substrate. This phenomenon could be due to the imperfection of the interface between the AgNW/PDMS composite film and the Eco-flex substrate. Though the blisters occur at random locations, the final configuration tends to be the same, with the almost uniformly distributed periodic structure in terms of both amplitude and wavelength. In Figure 2a, we can see that the gaps between the blisters show a very interesting self-adjusting behavior: the 2nd and 3rd blisters tend to come closer and the 6th blister moves left to give way to the growing 7th blister. Figure 2b shows the side view of buckle-delamination evolution of a typical blister under the increasing compressive strain. It can be seen that the blister amplitude keeps increasing, while the wavelength increases first then decreases under further compression. Such a selfadjusting behavior is effective in mitigating the local strain concentration, which contributes to achieving larger stretchability. Note that the initial position of each delaminated buckle could vary if we stretch the substrate to the prestrain and release it again. But with self-adjusting, the final configurations are close. Moreover, the resistance vs. the applied strain (e.g., Figure 4a) exhibits nearly the same behavior. Therefore, for the purpose of a stretchable conductor, the spontaneous buckle-delamination with selfadjusting is a reliable process.

Figure 3a shows that the evolution of blisters includes three stages, in terms of wavelength δ and amplitude h, with respect

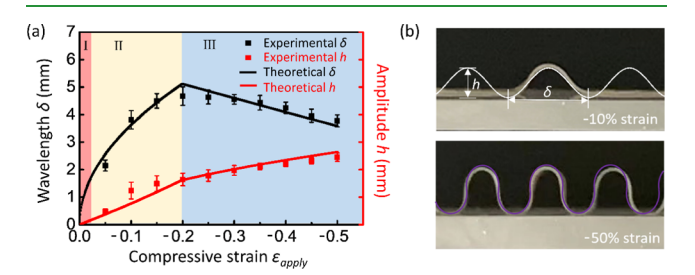


Figure 3. (a) Theoretical and experimental results of wavelength and amplitude of blisters under compressive strain from 0 to -50%. (b) Comparison between the theoretical profiles and experimental photographs of the cross-section view of blisters under -10% strain and -50% strain.

to the compressive strain. We assume that the film is inextensible and the membrane strain is negligible during deformation. The thickness of the Eco-flex substrate was over 100 times larger than that of the composite film. In our work, the thickness of Eco-flex showed no effect on the buckling behavior. Therefore, Eco-flex was considered infinitely thick in the analysis.

Stage I: when the compressive strain is beyond the critical wrinkle strain $\varepsilon_{\rm cw}=-(3\bar{E}_{\rm s}/\bar{E}_{\rm f}))^{2/3}/4$, where $\bar{E}_{\rm f}$ and $\bar{E}_{\rm s}$ are the effective Young's modulus calculated by $E_{\rm f}/(1+\nu_{\rm f}^2)$ and $E_{\rm s}/(1+\nu_{\rm s}^2)$ with $E_{\rm f}$ $\nu_{\rm f}$ $E_{\rm s}$, $\nu_{\rm s}$ being Young's modulus and Poisson's ratio of the AgNW/PDMS composite film and Eco-flex substrate. The critical wrinkle strain $\varepsilon_{\rm cw}$ is typically very small, predicted to be -2.1% in our case, which was not observed in our experiment. With the increasing compression, the wrinkle amplitude grows, thus delamination may occur as a result of increasing normal and shear forces at the interface. At the critical delamination strain $\varepsilon_{\rm cd}$, the first blister delaminates from the substrate overcoming the interfacial fracture toughness. The relationship between and is given as $\varepsilon_{\rm cd} = \varepsilon_{\rm cw} - (3 - 4\nu_{\rm s})^2(\sigma_{\rm max}/E_{\rm s})^2/[16(1-\nu_{\rm s})^4]$, where $\sigma_{\rm max}$ is the maximum

stress between the AgNW/PDMS composite film and Eco-flex (interfacial strength). ^{29,36} In our experiment, the onset of delamination was observed to occur at -4.3%, which agrees reasonably well with theoretical prediction $\varepsilon_{cd} = -4.1\%$.

Stage II starts with the first blister popping up and delaminating from the substrate. The evolution of blisters still follows the shape of a sinusoidal function that can be described by

$$w = \frac{h}{2} \left[1 + \cos \left(\frac{2\pi x}{\delta} \right) \right] \tag{1}$$

where δ and h are the wavelength and amplitude of the blister, respectively. Using an energy-based mechanical model developed by Zhang and Yin,³² the solutions of δ and h in this stage are given as

$$\begin{cases} \delta = \pi t \sqrt{\frac{\overline{E_f}t}{\Gamma}} \sqrt{\varepsilon_{\text{apply}}} \\ h = 2t \sqrt{\frac{\overline{E_f}t}{\Gamma}} \frac{\varepsilon_{\text{apply}}}{\sqrt{1 - \varepsilon_{\text{apply}}}} \end{cases}$$
(2)

where t is the thickness of the upper film, $\overline{E}_{\rm f}$ is the effective Young's modulus defined by $E_{\rm f}/(1+v_{\rm f}^2)$ with $E_{\rm f}$ and $v_{\rm f}$ Young's modulus and Poisson's ratio of the AgNW/PDMS composite film, is the compressive strain, and Γ is the interfacial toughness that can be measured (e.g., by the peel test).³⁷ Note that considering the AgNW/PDMS composite layer is much thinner than the pure PDMS layer (thickness ratio of 3:100), Young's modulus and Poisson's ratio of PDMS were used for the AgNW/PDMS composite film.

In Figure 3a, we can observe a drop in the wavelength of the blister after \sim -20% compressive strain in the experiment, which conflicts with the wavelength evolution predicted by eq 2. This is due to the limitation of the sinusoidal assumption in the model. This indicates the emergence of a new stage (stage III) and a new model would be needed.

In stage III, the number of the periodic blisters remains unchanged as observed from the experiment, while the wavelength of the blisters starts to decrease with increasing strain. The wavelength of the blister was found to linearly decrease with the increasing applied strain, as given by

$$\delta = \delta_{\text{max}} (1 - \varepsilon_{\text{apply}}) / (1 - \varepsilon_{\text{T}})$$
(3)

where $\delta_{\rm max}$ is the maximum wavelength of the blister when the applied strain reaches $\varepsilon_{\rm T}$, which is the transition strain between stage II and stage III. In this experiment, the transition strain was found to be around -20%.

Since the delamination stops growing during stage III, the blisters are under pure bending with both ends of each blister fixed. Thus, it becomes an elastica problem.³⁸ The blister wavelength and amplitude are given by³²

$$\begin{cases} \delta(s) = -s + \frac{2}{\alpha} E[am(\alpha s, \sin(\overline{\theta}/2)), \sin(\overline{\theta}/2)] \\ h(s) = \frac{2\sin(\overline{\theta}/2)}{\alpha} [1 - cn(\alpha s)] \end{cases}$$
(4)

where $\theta(s)$ is defined as the rotation field along the curvilinear coordinate $s \in (-l/2, l/2)$ and $\overline{\theta} = \theta(-l/4)$ is the rotation angle at 1/4 length of a blister length, E(,) is the incomplete elliptic integrals of the second kind, am and cn are the Jacobi

amplitude and the Jacobi cosine amplitude functions, respectively. α is a dimensionless parameter determined by the angle of rotation.³⁶

Figure 3a shows the comparison between theoretical predictions and experimental measurements of both h and δ . The experimental results start when the pop-up of the first blister was observed. The theoretical h and δ are derived from eq 2 in stage II and eq 4 in stage III, respectively. For both stages II and III, the experimental and theoretical results agree well. Figure 3b shows the comparison between the experiment and theory on the cross-sectional profiles when the applied strain was -10% (stage II with sinusoidal function) and -50% (stage III with elastica function), where the predicted profiles are overlaid on top of the images. After releasing the prestrain, the as-fabricated stretchable conductor has an average wavelength of 3.772 mm and an amplitude of 2.457 mm, which agrees well with theoretical predictions.

The buckle-delaminated AgNW/PDMS composite film can be used as a stretchable conductor. Figure 4a shows the relative

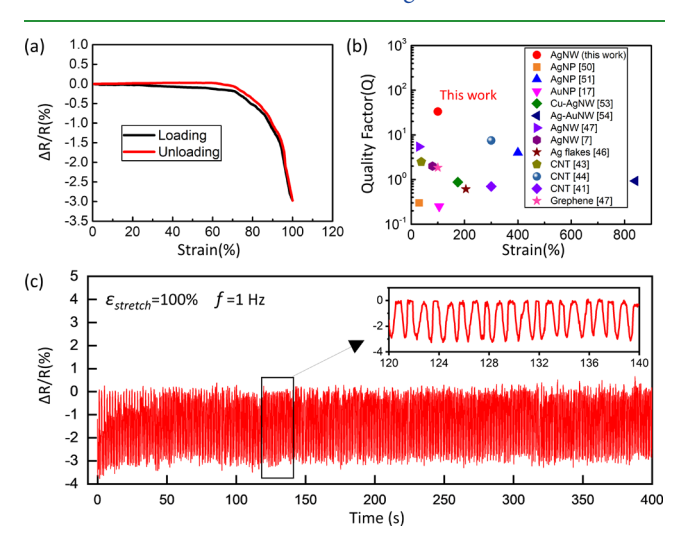


Figure 4. (a) Resistance change of the conductor under 100% stretching (loading and unloading) with respect to applied stretching strain. (b) Comparison of this work to recent works in stretchable conductors.^{7,17,41,43,44,47,50–54} (c) Resistance change of the conductor under 1 Hz, 100% strain cycle loading.

resistance change of the film with respect to the applied tensile strain. It can be seen that the relative resistance decreased slightly with the increasing tensile strain (\sim 3% decrease in resistance corresponding to 100% tensile strain), and that the resistance change was totally reversible according to the loading and unloading responses. In general, buckle-delamination significantly reduces the strain in the buckled film, but

there is a still small compressive strain in the film. The delaminated buckles are in the form of sinewave (stage II) or elastica (stage III), which can be approximated as bending with some parts (e.g., peaks) in tension and some parts (e.g., valleys) in compression. Their effect on the resistance change can be largely canceled out. In addition to the bending strain, a compressive membrane strain exists across the entire film.³¹ The compressive strain, even small, can alter the AgNW percolation network, leading to an increase in the resistance. When stretching the buckle-delaminated AgNW/PDMS composite film, the (small) compressive strain is released all of the way to zero, which is responsible for the slight resistance decrease as observed. Figure 4c shows the resistance change of the film under 400 cycles of loading and unloading at 1 Hz frequency and 100% strain. It can be seen that the resistance change is totally reversible.

An ideal stretchable conductor should maintain constant conductance irrespective of the applied strain, which is however very challenging. A large variety of nanomaterials have been explored as stretchable conductors such as carbon nanotubes (CNTs),^{6,11,40-44} graphene,⁴⁵⁻⁴⁷ silver/gold nanoparticles,^{17,48-51} and metal nanowires.^{7,22,52-54} However, they all showed a trade-off between stretchability and quality factor (Q, the percent strain divided by the percent resistance change). Figure 4b plots the quality factor with respect to the stretchability of the representative nanomaterial-enabled stretchable conductors. For example, a Ag-Au nanowirebased stretchable conductor reported by Kim et al. can be stretched to 840%, but the quality factor is less than 1.54 A silver nanowire integrated with textile structure has been reported with a quality factor of around 5.45, while the strain range is less than 30%. 52 In this work, the quality factor reached 33.3 with the strain range of 100%. Of note is that, for almost all of the reported stretchable conductors, the resistance increases with the increasing tensile strain. By contrast, in our case, the resistance slightly decreases, which could be potentially conducive for certain applications. Under further stretching, the AgNW/PDMS composite film will be under tensile strain and the resistance will increase quickly and jump to infinity at approximately 110% strain. Hence, the effective stretchable range of our buckle-delaminated AgNW/PDMS film is 100% tensile strain.

For wearable sensors, a major challenge is the interconnection between the sensing units and front-end electronics (e.g., data acquisition and transmission modules). Since our stretchable conductor maintained nearly constant conductance under large strain, we developed an integrated sensor/conductor module, as shown in Figure 5a. First, two ribbons of the AgNW/PDMS composite film were prepared using the same fabrication method reported earlier in this paper. One

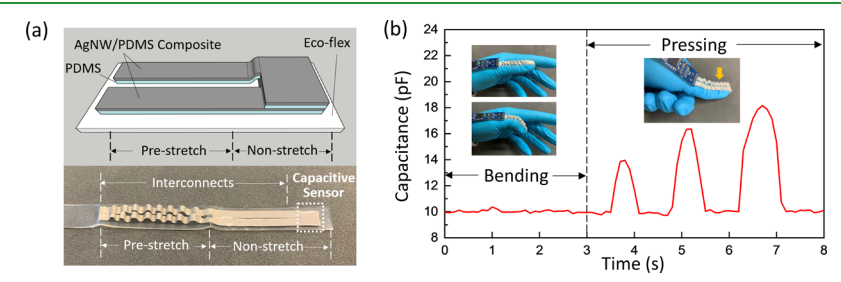


Figure 5. (a) Schematic illustration and photograph of the integrated sensor-conductor module. (b) Capacitance changes of the integrated sensor-conductor module attached on a thumb that bends and presses.

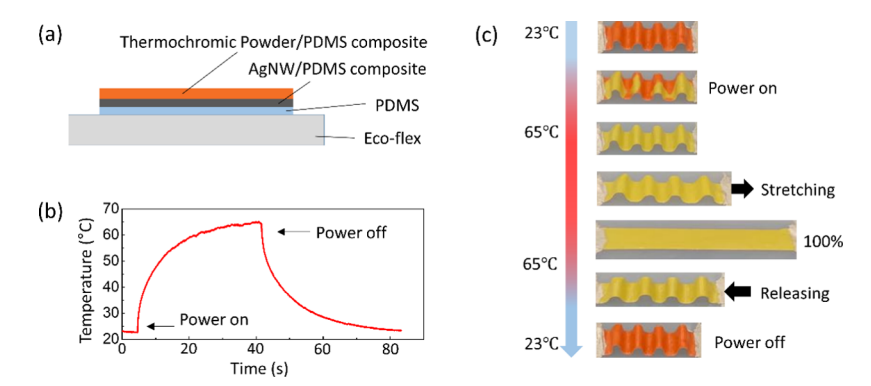


Figure 6. (a) Schematic view on the cross section of the stretchable thermochromic conductor. (b) Temperature change of the stretchable thermochromic conductor when powered with 2 V voltage and then turn off the power. (c) Photographs of the stretchable thermochromic conductor changing color: First heat up the stretchable conductor with 2 V direct current resulting in a temperature rise from 23 to ~65 °C, stretch the conductor to 100% strain and release, finally turn off the power and cool down to original room temperature.

end of each ribbon extended to a square-shaped pad that overlapped with each other, while the other ends were placed side by side. Then, the Eco-flex substrate was partially prestretched (including both prestretch and nonstretch parts) before the AgNW/PDMS composite ribbons were transferred on top. Then, the prestretched part of the substrate was released, resulting in uniformly distributed buckle-delamination structure of the AgNW/PDMS composite ribbons. The AgNW/PDMS composite ribbons on the nonstretched part were attached to the substrate to complete a parallel capacitor (a capacitive pressure sensor). The capacitive sensor can detect the strain (up to \sim 50%), pressure (up to \sim 1.2 MPa) with fast response time (~40 ms). 55 As shown in Figure 5b, the integrated sensor/conductor module was attached to the back and pulp of a thumb, with one end connected to a PCB (on the back of the thumb) and the other end (the capacitive sensor) wrapped over to the thumb pulp. In the first three seconds, the thumb bent and recovered in the air with constant capacitance, which indicates that deformation of the stretchable conductors did not interfere with the capacitance measurement. Subsequently, the thumb pressed on a rigid object three times with increasing pressure, and an increasing change of capacitance was observed.

AgNW-based stretchable heaters have been reported recently, 56-58 which can be used in a variety of applications such as thermal treatment, bimorph actuator, and thermo-chromic devices. 52,57,59 Here, we report a reversible colorchanging stretchable conductor that can switch between two colors at a very low voltage. The conductor was a sandwiched structure containing three layers, as illustrated in Figure 6a. The top layer, the thermochromic layer, was prepared by mixing red chromic powder and yellow acrylic paint together with the PDMS precursor and then cured in an oven. The middle layer and bottom layer were prepared together using the same drop-casting and peeling off methods, as described in the fabrication of the AgNW/PDMS composite film. The two ends of the multilayer stripe were fixed and connected to a copper wire by silver epoxy. As shown in Figure 6b, when applied with the DC power supply, the temperature on the stretchable conductor rose quickly due to the Joule heating effect of the AgNWs. The thermochromic powder is originally red at room temperature (23 °C) and turns transparent at a temperature over 35 °C. As shown in Figure 6c, the initial color of the conductor was a mixture of red and yellow, i.e., orange, at room temperature. With the Joule heating, the

temperature rose to 64.8 ± 0.7 °C (Figure S3). The red thermochromic powder inside gradually faded away and the remaining yellow acrylic paint was revealed. The response time of the thermochromic pigment is within 2 s. Multiple stretching and releasing cycles (up to 100% strain) did not affect the heating temperature because the buckle-delamination structure provided the excellent stretchability. The colorchanging performance of the thermochromic heater remained stable and consistent after 100 cycles (Figure S1). Finally, when the power was turned off, temperature on the composite film dropped back to room temperature and the thermochromic layer appeared orange again. This stretchable thermochromic conductor can be applied to wearable thermal therapy devices for warning of over heat.

CONCLUSIONS

A novel stretchable AgNW conductor was reported in this paper, where a highly conductive AgNW/PDMS composite film served as the conducting material, while the buckledelamination structure-enabled excellent stretchability (demonstrated up to 100%). Due to the spontaneous out-of-plane deformation as a result of the buckle-delamination, the local strain in the AgNW/PDMS composite layer was significantly reduced. The spontaneous buckle-delamination was found to pop-up at random locations but exhibited an interesting selfadjusting behavior, leading to a uniform distribution of the blisters. As a result, the resistance change of our stretchable conductor was within 3% under a stretching to 100%. Geometry evolution of the delaminated buckles was captured in real time, which agreed well with the theoretical analysis. The potential applications of this stretchable conductor were demonstrated with an integrated sensor/conductor module and a color-changing thermochromic device. The fabrication process for the reported stretchable conductor is simple and scalable. Overall, this work highlights the important relevance of the mechanics-based design in the nanomaterial-enabled stretchable devices.

METHODS

Materials. PVP (MW $\sim 40\,000$), CuCl $_2$ (CuCl $_2\cdot 2H_2O$, >99.999%), and AgNO $_3$ (>99%) were bought from Sigma-Aldrich, Co. PDMS (SYLGARD 184) was bought from DOW Inc. Eco-flex (00–30) was bought from Smooth-On, Inc. Silver epoxy was bought from MG Chemicals Co. The thermochromic pigment was bought from Knock Out Chemicals Inc.

Fabrication of Stretchable AgNW Conductors. For a typical synthesis, a modified polyol process was used. First, 60 mL of a 0.147 M PVP (MW ~ 40 000, Sigma-Aldrich) solution in EG (was added to a round-bottom flask to which a stir bar was added; the vial was then suspended in an oil bath (temperature 151.5 °C) and heated for 1 h under magnetic stirring (150 rpm). Then, at 1 h, 200 μ L of a 24 M CuCl₂ (CuCl₂·2H₂O, >99.999%, Sigma-Aldrich) solution in EG was injected into the PVP solution. The solution was then heated for an additional 15 min, followed by injecting 60 mL of a 0.094 M AgNO₃ (>99%, Sigma-Aldrich) solution in EG. AgNWs in ethanol solution with an average diameter of 90 nm and length of 20-30 μm were shaken for 5 min before use to disperse the nanowires in the solution. The AgNW solution was drop-casted on the plasma-treated tattoo paper; at the same time, the solution was heated by a hot plate at 50 °C to evaporate the solvent. After the evaporation of ethanol, the patterned AgNWs were thermally annealed at 150 °C for 20 min. Then, liquid PDMS (SYLGARD 184) with a weight ratio of 10:1 was spin-coated onto the AgNW film, degassed, and subsequently thermally cured at 100 °C for 1 h. For the substrate, we used Ecoflex 00-30 (Smooth-on) with a weight ratio of 1:1. The substrate was naturally cured in room temperature for 24 h and cut into the desired shape. Then, the AgNW/PDMS composite film was transfer-printed onto a prestretched Eco-flex substrate by washing off the tattoo paper with water. Finally, simply releasing the prestrain on the substrate gives the upper film a sinusoidal shaped buckle-delamination structure. Cu wires were attached to the two ends of the conductor by silver epoxy (MG Chemicals) for connection to the power source.

Fabrication of Stretchable Thermochromic Conductors. To add a layer of the temperature-sensitive color-changing layer, we first spin coat a layer of liquid PDMS (SYLGARD 184) with thermochromic powder mixed inside onto the tattoo paper. To increase contrast during color changing, we also added some yellow acrylic paint together with red thermochromic powder forming an orange color as the initial state. The thermal chromic powder is red in room temperature (23 °C) and becomes transparent when the temperature rises to ~35 °C. Then, the AgNW/PDMS composite film was fabricated on top of the thermochromic PDMS layer. The rest of the fabrication procedures is exactly the same as discussed in the fabrication of the AgNW conductor.

Measurements. The resistance change of the stretchable conductor was measured by a digital multimeter (34401A Agilent) with errors of 0.0035% DC and 0.06% AC. The capacitance of the sensor/conductor module was measured by a capacitance reader (FDC1004 Texas Instrument) with an error of ± 6 fF. A temperature change of the stretchable thermochromic heater was measured with an infrared camera (A655SC FLIR) with an error of ± 2 °C or ± 2 % of reading.

ASSOCIATED CONTENT

Supporting Information

The Supporting Information is available free of charge at https://pubs.acs.org/doi/10.1021/acsami.0c09775.

Photographs showing the color change of the stretchable thermochromic heater under the 1st cycle and 100th cycle of 2 V Joule heating; capacitance change with respect to applied pressure on the integrated sensor-conductor module; temperature changes of five different locations on the stretchable thermal chromic heater under 2 V Joule heating versus time (PDF)

AUTHOR INFORMATION

Corresponding Author

Yong Zhu — Department of Mechanical and Aerospace Engineering, North Carolina State University, Raleigh, North Carolina 27695, United States; Joint Department of Biomedical Engineering, University of North Carolina—Chapel Hill and NC State University, Chapel Hill, North Carolina 27599, *United States;* orcid.org/0000-0002-3862-5757; Email: yong zhu@ncsu.edu

Authors

Shuang Wu — Department of Mechanical and Aerospace Engineering, North Carolina State University, Raleigh, North Carolina 27695, United States

Shanshan Yao — Department of Mechanical and Aerospace Engineering, North Carolina State University, Raleigh, North Carolina 27695, United States; Oorcid.org/0000-0002-2076-162X

Yuxuan Liu – Department of Mechanical and Aerospace Engineering, North Carolina State University, Raleigh, North Carolina 27695, United States

Xiaogang Hu – Joint Department of Biomedical Engineering, University of North Carolina—Chapel Hill and NC State University, Chapel Hill, North Carolina 27599, United States

He Helen Huang – Joint Department of Biomedical Engineering, University of North Carolina—Chapel Hill and NC State University, Chapel Hill, North Carolina 27599, United States

Complete contact information is available at: https://pubs.acs.org/10.1021/acsami.0c09775

Note:

The authors declare no competing financial interest.

ACKNOWLEDGMENTS

The authors gratefully acknowledge the financial support from the National Science Foundation (NSF) through Award no. IIS-1637892.

REFERENCES

- (1) Chortos, A.; Liu, J.; Bao, Z. Pursuing Prosthetic Electronic Skin. *Nat. Mater.* **2016**, *15*, 937–950.
- (2) Yao, S.; Swetha, P.; Zhu, Y. Nanomaterial-Enabled Wearable Sensors for Healthcare. *Adv. Healthcare Mater.* **2018**, 7, No. 1700889.
- (3) Roh, E.; Hwang, B.-U.; Kim, D.; Kim, B.-Y.; Lee, N.-E. Stretchable, Transparent, Ultrasensitive, and Patchable Strain Sensor for Human—Machine Interfaces Comprising a Nanohybrid of Carbon Nanotubes and Conductive elastomers. *ACS Nano* **2015**, *9*, 6252–6261
- (4) Rogers, J. A.; Someya, T.; Huang, Y. G. Materials and Mechanics for Stretchable Electronics. *Science* **2010**, *327*, 1603–1607.
- (5) Wang, C.; Wang, C.; Huang, Z.; Xu, S. Materials and Structures Toward Soft Electronics. *Adv. Mater.* **2018**, *30*, No. 1801368.
- (6) Chun, K.-Y.; Oh, Y.; Rho, J.; Ahn, J.-H.; Kim, Y.-J.; Choi, H. R.; Baik, S. Highly Conductive, Printable and Stretchable Composite Films of Carbon Nanotubes and Silver. *Nat. Nanotechnol.* **2010**, *5*, 853–857.
- (7) Xu, F.; Zhu, Y. Highly Conductive and Stretchable Silver Nanowire Conductors. *Adv. Mater.* **2012**, *24*, 5117–5122.
- (8) Yao, S.; Zhu, Y. Nanomaterial-Enabled Stretchable Conductors: Strategies, Materials and Devices. *Adv. Mater.* **2015**, *27*, 1480–1511.
- (9) Park, M.; Park, J.; Jeong, U. Design of Conductive Composite Elastomers for Stretchable Electronics. *Nano Today* **2014**, *9*, 244–260.
- (10) Liu, Z. F.; Fang, S.; Moura, F.; Ding, J.; Jiang, N.; Di, J.; Zhang, M.; Lepró, X.; Galvao, D.; Haines, C.; Yuan, N.; Yin, S.; Lee, D.; Wang, R.; Wang, H.; Lv, W.; Dong, C.; Zhang, R.; Chen, M.; Yin, Q.; Chong, Y.; ZHang, R.; Wang, X.; Lima, M.; Ovalle-Robles, R.; Qian, D.; Lu, H.; Baughman, R. Hierarchically Buckled Sheath-Core Fibers for Superelastic Electronics, Sensors, and Muscles. *Science* **2015**, *349*, 400–404.

- (11) Xu, F.; Wang, X.; Zhu, Y.; Zhu, Y. Wavy Ribbons of Carbon Nanotubes for Stretchable Conductors. *Adv. Funct. Mater.* **2012**, 22, 1279–1283.
- (12) Lipomi, D. J.; Vosgueritchian, M.; Tee, B. C.; Hellstrom, S. L.; Lee, J. A.; Fox, C. H.; Bao, Z. Skin-Like Pressure and Strain Sensors Based on Transparent Elastic Films of Carbon Nanotubes. *Nat. Nanotechnol.* **2011**, *6*, 788–792.
- (13) Jiang, H.; Khang, D. Y.; Song, J.; Sun, Y.; Huang, Y.; Rogers, J. A. Finite Deformation Mechanics in Buckled Thin Films on Compliant Supports. *Proc. Natl. Acad. Sci. USA* **2007**, *104*, 15607–15612
- (14) Cheng, H.; Song, J. A Simply Analytic Study of Buckled Thin Films on Compliant Substrates. J. Appl. Mech. 2013, 81, No. 024501.
- (15) Khang, D.-Y.; Jiang, H.; Huang, Y.; Rogers, J. A. A Stretchable Form of Single-Crystal Silicon for High-Performance Electronics on Rubber Substrates. *Science* **2006**, *311*, 208–212.
- (16) Dickey, M. D. Stretchable and Soft Electronics Using Liquid Metals. *Adv. Mater.* **2017**, *29*, No. 1606425.
- (17) Kim, Y.; Zhu, J.; Yeom, B.; Di Prima, M.; Su, X.; Kim, J.-G.; Yoo, S. J.; Uher, C.; Kotov, N. A. Stretchable Nanoparticle Conductors with Self-Organized Conductive Pathways. *Nature* **2013**, *500*, 59–63.
- (18) Gong, S.; Schwalb, W.; Wang, Y.; Chen, Y.; Tang, Y.; Si, J.; Shirinzadeh, B.; Cheng, W. A Wearable and Highly Sensitive Pressure Sensor with Ultrathin Gold Nanowires. *Nat. Commun.* **2014**, *5*, 1–8.
- (19) Hao, C.; Yang, B.; Wen, F.; Xiang, J.; Li, L.; Wang, W.; Zeng, Z.; Xu, B.; Zhao, Z.; Liu, Z.; Tian, Y. Flexible All-Solid-State Supercapacitors Based on Liquid-Exfoliated Black-Phosphorus Nanoflakes. *Adv. Mater.* **2016**, *28*, 3194–3201.
- (20) Cong, H.; Ren, X.; Wang, P.; Yu, S. Flexible Graphene—Polyaniline Composite Paper for High-Performance Supercapacitor. *Energy Environ. Sci.* **2013**, *6*, 1185–1191.
- (21) Huang, Q.; Zhu, Y. Printing Conductive Nanomaterials for Flexible and Stretchable Electronics: A Review of Materials, Processes, and Applications. *Adv. Mater. Technol.* **2019**, *4*, No. 1800546.
- (22) Lee, P.; Lee, J.; Lee, H.; Yeo, J.; Hong, S.; Nam, K. H.; Lee, D.; Lee, S. S.; Ko, S. H. Highly Stretchable and Highly Conductive Metal Electrode by Very Long Metal Nanowire Percolation Network. *Adv. Mater.* **2012**, *24*, 3326–3332.
- (23) Ge, J.; Yao, H.; Wang, X.; Ye, Y.; Wang, J.; Wu, Z.; Liu, J.; Fan, F.; Gao, H.; Zhang, C.; Yu, S. Stretchable Conductors Based on Silver Nanowires: Improved Performance through a Binary Network Design. *Angew. Chem., Int. Ed.* **2013**, *52*, 1654–1659.
- (24) Xue, Z.; Song, H.; Rogers, J. A.; Zhang, Y.; Huang, Y. Mechanically-Guided Structural Designs in Stretchable Inorganic Electronics. *Adv. Mater.* **2020**, 32, No. 1902254.
- (25) Zhang, Y.; Yan, Z.; Nan, K.; Xiao, D.; Liu, Y.; Luan, H.; Fu, H.; Wang, X.; Yang, Q.; Wang, J.; Ren, W.; Si, H.; Liu, F.; Yang, L.; Li, H.; Wang, J.; Guo, X.; Luo, H.; Wang, L.; Huang, Y.; John, A. R. A Mechanically Driven Form of Kirigami as a Route to 3D Mesostructures in Micro/Nanomembranes. *Proc. Natl. Acad. Sci. USA* 2015, 112, 11757–11764.
- (26) Zhang, Y.; Wang, S.; Li, X.; Fan, J. A.; Xu, S.; Song, Y. M.; Choi, K.-J.; Yeo, W.-H.; Lee, W.; Nazaar, S. N.; Lu, B.; Yin, L.; Hwang, K.-C.; Rogers, J. A.; Huang, Y. Experimental and Theoretical Studies of Serpentine Microstructures Bonded To Prestrained Elastomers for Stretchable Electronics. *Adv. Funct. Mater.* **2014**, *24*, 2028–2037.
- (27) Sun, Y.; Choi, W. M.; Jiang, H.; Huang, Y.; Rogers, J. A. Controlled Buckling of Semiconductor Nanoribbons for Stretchable Electronics. *Nat. Nanotechnol.* **2006**, *1*, 201–207.
- (28) Xu, F.; Lu, W.; Zhu, Y. Controlled 3D Buckling of Silicon Nanowires for Stretchable Electronics. ACS Nano 2011, 5, 672–678.
- (29) Mei, H.; Landis, C. M.; Huang, R. Concomitant Wrinkling and Buckle-Delamination of Elastic Thin Films on Compliant Substrates. *Mech. Mater.* **2011**, *43*, 627–642.
- (30) Jiang, H.; Sun, Y.; Rogers, J. A.; Huang, Y. Post-Buckling Analysis for the Precisely Controlled Buckling of Thin Film Encapsulated by Elastomeric Substrates. *Int. J. Solids Struct.* **2008**, 45, 2014–2023.

- (31) Thomas, A. V.; Andow, B. C.; Suresh, S.; Eksik, O.; Yin, J.; Dyson, A. H.; Koratkar, N. Controlled Crumpling of Graphene Oxide Films for Tunable Optical Transmittance. *Adv. Mater.* **2015**, 27, 3256–3265.
- (32) Zhang, Q.; Yin, J. Spontaneous Buckling-Driven Periodic Delamination of Thin Films on Soft Substrates under Large Compression. *J. Mech. Phys. Solids* **2018**, *118*, 40–57.
- (33) Jiang, H.; Sun, Y.; Rogers, J. A.; Huang, Y. Mechanics of Precisely Controlled Thin Film Buckling on Elastomeric Substrate. *Appl. Phys. Lett.* **2007**, *90*, No. 133119.
- (34) Zhang, Q.; Tang, Y.; Hajfathalian, M.; Chen, C.; Turner, K. T.; Dikin, D. A.; Lin, G.; Yin, J. Spontaneous Periodic Delamination of Thin Films to Form Crack-Free Metal and Silicon Ribbons with High Stretchability. *ACS Appl. Mater. Interfaces* **2017**, *9*, 44938–44947.
- (35) Vella, D.; Bico, J.; Boudaoud, A.; Roman, B.; Reis, P. M. The Macroscopic Delamination of Thin Films from Elastic Substrates. *Proc. Natl. Acad. Sci. USA* **2009**, *106*, 10901–10906.
- (36) Bowden, N.; Brittain, S.; Evans, A. G.; Hutchinson, J. W.; Whitesides, G. M. Spontaneous Formation of Ordered Structures in Thin Films of Metals Supported on an Elastomeric Polymer. *Nature* **1998**, 393, 146–149.
- (37) Volinsky, A.; Moody, N.; Gerberich, W. Interfacial Toughness Measurements for Thin Films on Substrates. *Acta Mater.* **2002**, *50*, 441–466.
- (38) Wagner, T. J.; Vella, D. The 'Sticky Elastica': Delamination Blisters beyond Small Deformations. *Soft Matter* **2013**, *9*, 1025–1030. (39) Song, J.; Jiang, H.; Liu, Z. J.; Khang, D. Y.; Huang, Y.; Rogers, J. A.; Lu, C.; Koh, C. G. Buckling of a Stiff Thin Film on a Compliant Substrate in Large Deformation. *Int. J. Solids Struct.* **2008**, *45*, 3107–3121.
- (40) Zhu, Y.; Xu, F. Buckling of Aligned Carbon Nanotubes as Stretchable Conductors: A New Manufacturing Strategy. *Adv. Mater.* **2012**, *24*, 1073–1077.
- (41) Shin, M. K.; Oh, J.; Lima, M.; Kozlov, M. E.; Kim, S. J.; Baughman, R. H. Elastomeric Conductive Composites Based on Carbon Nanotube Forests. *Adv. Mater.* **2010**, *22*, 2663–2667.
- (42) Yamada, T.; Hayamizu, Y.; Yamamoto, Y.; Yomogida, Y.; Izadi-Najafabadi, A.; Futaba, D. N.; Hata, K. A Stretchable Carbon Nanotube Strain Sensor for Human-Motion Detection. *Nat. Nanotechnol.* **2011**, *6*, 296–301.
- (43) Kim, J. H.; Hwang, J.-Y.; Hwang, H. R.; Kim, H. S.; Lee, J. H.; Seo, J.-W.; Shin, U. S.; Lee, S.-H. Simple and Cost-Effective Method of Highly Conductive and Elastic Carbon Nanotube/Polydimethylsiloxane Composite for Wearable Electronics. *Sci. Rep.* **2018**, *8*, 1–11.
- (44) Wang, P.; Peng, Z.; Li, M.; Wang, Y. Stretchable Transparent Conductive Films from Long Carbon Nanotube Metals. *Small* **2018**, *14*, No. 1802625.
- (45) Xu, Z.; Liu, Z.; Sun, H.; Gao, C. Highly Electrically Conductive Ag-Doped Graphene Fibers as Stretchable Conductors. *Adv. Mater.* **2013**, 25, 3249–3253.
- (46) Chen, Z.; Ren, W.; Gao, L.; Liu, B.; Pei, S.; Cheng, H. Three-Dimensional Flexible and Conductive Interconnected Graphene Networks Grown by Chemical Vapour Deposition. *Nat. Mater.* **2011**, *10*, 424–428.
- (47) Liu, N.; Chortos, A.; Lei, T.; Jin, L.; Kim, T. R.; Bae, W.-G.; Zhu, C.; Wang, S.; Pfattner, R.; Chen, X.; Sinclair, R.; Bao, Z. Ultratransparent and Stretchable Graphene Electrodes. *Sci. Adv.* **2017**, 3, No. e1700159.
- (48) Park, M.; Im, J.; Shin, M.; Min, Y.; Park, J.; Cho, H.; Park, S.; Shim, M.-B.; Jeon, S.; Chung, D.-Y.; Bae, J.; Park, J.; Jeong, U.; Kim, K. Highly Stretchable Electric Circuits from a Composite Material of Silver Nanoparticles and Elastomeric Fibres. *Nat. Nanotechnol.* **2012**, *7*, 803–809.
- (49) Matsuhisa, N.; Kaltenbrunner, M.; Yokota, T.; Jinno, H.; Kuribara, K.; Sekitani, T.; Someya, T. Printable Elastic Conductors with a High Conductivity for Electronic Textile Applications. *Nat. Commun.* **2015**, *6*, No. 7461.
- (50) Zhang, S.; Li, Y.; Tian, Q.; Liu, L.; Yao, W.; Chi, C.; Zeng, P.; Zhang, N.; Wu, W. Highly Conductive, Flexible and Stretchable

Conductors Based on Fractal Silver Nanostructures. J. Mater. Chem. C 2018, 6, 3999–4006.

- (51) Matsuhisa, N.; Inoue, D.; Zalar, P.; Jin, H.; Matsuba, Y.; Itoh, A.; Yokota, T.; Hashizume, D.; Someya, T. Printable Elastic Conductors by In Situ Formation of Silver Nanoparticles from Silver Flakes. *Nat. Mater.* **2017**, *16*, 834–840.
- (52) Yao, S.; Yang, J.; Poblete, F. R.; Hu, X.; Zhu, Y. Multifunctional Electronic Textiles Using Silver Nanowire Composites. *ACS Appl. Mater. Interfaces* **2019**, *11*, 31028–31037.
- (53) Catenacci, M. J.; Reyes, C.; Cruz, M. A.; Wiley, B. J. Stretchable Conductive Composites from Cu–Ag Nanowire Felt. *ACS Nano* **2018**, *12*, 3689–3698.
- (54) Choi, S.; Han, S. I.; Jung, D.; Hwang, H. J.; Lim, C.; Bae, S.; Park, O. K.; Tschabrunn, C. M.; Lee, M.; Bae, S. Y.; Yu, J. W.; Ryu, J. H.; Lee, S. W.; Park, K. P.; Kang, P. M.; Lee, W. B.; Nezafat, R.; Hyeon, T.; Kim, D. H. Highly Conductive, Stretchable and Biocompatible Ag—Au Core—Sheath Nanowire Composite for Wearable and Implantable Bioelectronics. *Nat. Nanotechnol.* **2018**, *13*, 1048–1056.
- (55) Yao, S.; Zhu, Y. Wearable Multifunctional Sensors Using Printed Stretchable Conductors Made of Silver Nanowires. *Nanoscale* **2014**, *6*, 2345–2352.
- (56) Choi, S.; Park, J.; Hyun, W.; Kim, J.; Kim, J.; Lee, Y. B.; Song, C.; Hwang, H. J.; Kim, J. H.; Hyeon, T.; Kim, D. H. Stretchable Heater Using Ligand-Exchanged Silver Nanowire Nanocomposite for Wearable Articular Thermotherapy. ACS Nano 2015, 9, 6626–6633.
- (57) Yao, S.; Cui, J.; Cui, Z.; Zhu, Y. Soft Electrothermal Actuators Using Silver Nanowire Heaters. *Nanoscale* **2017**, *9*, 3797–3805.
- (58) Hong, S.; Lee, H.; Lee, J.; Kwon, J.; Han, S.; Suh, Y. D.; Cho, H.; Shin, J.; Yeo, J.; Ko, S. H. Highly Stretchable and Transparent Metal Nanowire Heater for Wearable Electronics Applications. *Adv. Mater.* **2015**, 27, 4744–4751.
- (59) Jin, Y.; Lin, Y.; Kiani, A.; Joshipura, I. D.; Ge, M.; Dickey, M. D. Materials Tactile Logic via Innervated Soft Thermochromic Elastomers. *Nat. Commun.* **2019**, *10*, 1–8.